IEEE Access
Multidisciplinary | Rapid Review | Open Access Journal

Received June 24, 2017, accepted July 11, 2017, date of publication July 18, 2017, date of current version October 25, 2017.

*Digital Object Identifier 10.1109/ACCESS.2017.2727522*

# Non-Autonomous Second-Order Memristive Chaotic Circuit

**QUAN XU[1], QINLING ZHANG[1], BOCHENG BAO[1], AND YIHUA HU[2], (Senior Member, IEEE)**
[1]School of Information Science and Engineering, Changzhou University, Changzhou 213164, China
[2]Department of Electrical Engineering and Electronics, University of Liverpool, Liverpool L69 3GJ, U.K.

Corresponding author: Bocheng Bao (mervinbao@126.com)

This work was supported in part by the National Natural Science Foundation of China under Grant 61601062 and Grant 51607013 and in part by the Natural Science Foundations of Jiangsu Province, China, under Grant BK20160282.

**ABSTRACT** A non-autonomous second-order memristive chaotic circuit is considered in this paper, which is comparatively simple, only consisting of a memristor, a capacitor, a resistor, and a sinusoidal voltage source. Based on the descriptive equation of the memristive circuit, the dynamical behaviors are investigated by theoretical analyses and numerical simulations. It is noted that the number of AC equilibrium points changes with the evolution of the time and the circuit exhibits striking dynamical features, including period, chaos, forward period-doubling, reverse period-doubling, tangent bifurcation, and crisis scenarios. Furthermore, a hardware circuit is set up by off-the-shelf discrete components, where hardware experiments are performed to verify the numerical results. The most significant feature of the proposed memristive circuit is the inductor-free realization with simplified topology, which makes the circuit much simpler and more intuitive in physical realization.

**INDEX TERMS** Chaos, memristive circuit, non-autonomous.

## I. INTRODUCTION

As the fourth basic circuit element, memristor, described by flux and charge [1], brings completely new development space in various interdisciplinary areas. Specially, many researchers started to exploit memristor based application circuits due to the unique feature of memristor in the past few years [2]–[16]. Summarily, memristors with versatile nonlinearities are conveniently integrated into some existing linear or nonlinear electronic circuits to build various novel memristive chaotic circuits [17]. Some rich dynamical behaviors, such as chaos and hyperchaos [3], [4], hyperchaotic multi-wing attractors [2], [5], coexisting multiple attractors [6], [7], hidden attractors [8], complex transient chaos and hyperchaos [9]–[11], chaotic and hyperchaotic beats [10], [12], to mention a few, have been revealed from these memristive chaotic circuits and analyzed by numerical simulations and hardware experiments. However, due to technical drawbacks and high cost in fabricating nanoscale devices, most of the memristors in those application circuits are equivalently realized by operational amplifiers and analog multipliers [7], [8], [13], [14], as well as memristive diode bridges cascaded with RC, LC or RLC filters [6], [15], [16].

Nonlinear electronic circuits have attracted appreciable attention because they can provide powerful experimental and analytical platforms for people to understand dynamical behaviors in physics [18], engineering [19], [20], electronic [21] and neurology [22]. Considering that a simple nonlinear electronic circuit can serve as a paradigm for better understanding of bifurcation and chaos, it is a significant research topic to simplify chaotic circuits by minimizing the number of dynamic elements and physical components [23]–[27]. Statistically speaking, non-autonomous circuits, one of the main forms of chaotic circuits, contain fewer dynamic elements than autonomous chaotic circuits since externally driven signals can replace a dynamic element or an oscillating unit in autonomous chaotic circuits [25], [26]. Just like many autonomous chaotic circuits, non-autonomous nonlinear circuits can also exhibit many interesting dynamical phenomena [10]–[12].

However, in relevant literatures, most of those memristive chaotic circuits are at least fourth-order autonomous [15] or third-order non-autonomous [10], [12]. Additionally, when inductor-free realization without manually winding inductor is presented, the circuit can be regarded as a gadget, which is more suitable for IC design [27]–[29]. Motivated by those considerations, by replacing the passive LC filter with a standard sinusoidal voltage source in the existing memristive Chua's circuit [7], the simplest second-order non-autonomous inductor-free memristive circuit is proposed in this paper. Dynamical behaviors of limit cycles and strange

attractors are fortunately obtained by numerical simulations and hardware experiments. The aim of the present work is to reveal the unknown features in the proposed memristive chaotic circuit.

## II. NON-AUTONOMOUS MEMRISTIVE CIRCUIT

The schematic diagram of a new non-autonomous second-order memristive circuit and a memristor equivalent realization circuit are shown in Fig. 1. The proposed circuit is physically realizable and only consists of a capacitor $C_1$, a resistor $R$, a sinusoidal voltage source $v_s$, and a voltage-controlled $W$. Compared with the non-autonomous memristive circuits in [10]–[12], the newly proposed circuit is second-order and inductor-free realization with a simplified topological structure outstandingly. Also, the comparisons of some non-autonomous memrisitve chaotic circuits are given in Tab.1.

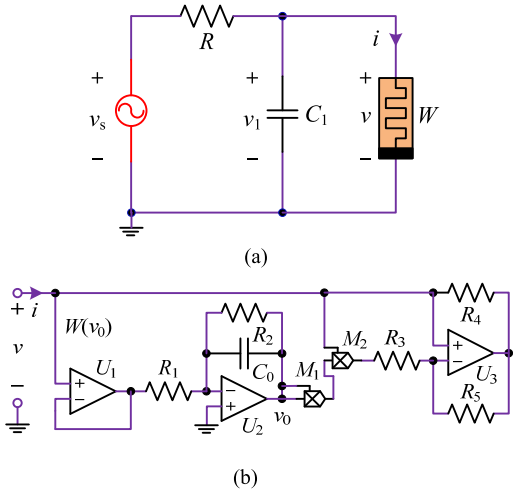


**FIGURE 1.** Second-order non-autonomous inductor-free memristive chaotic circuit. (a) Circuit schematic diagram. (b) Equivalent circuit of memristor.

**TABLE 1.** Comparison of non-autonomous memristive chaotic circuits.

| Items | Ref. [10] | Ref. [11] | Ref. [12] | Proposed circuit |
|---|---|---|---|---|
| Linear element | 1 capacitor<br>1 resistor<br>1 inductor | 2 capacitor<br>1 resistor<br>1 inductor | 2 capacitor<br>2 resistor<br>1 inductor | 1 capacitor<br>1 resistor |
| Memductance function | Piecewise linear | Absolute value | Piecewise linear | Quadratic |
| Complexity of emulator | Complex | Simple | Complex | Simple |
| Inductor-free | No | No | No | Yes |

Memristor is a nonlinear circuit element, which can be used to realize nonlinearity of the circuit in Fig. 1(a). According to [7], the equivalent realization circuit of the memristor is depicted in Fig. 1(b), which is mathematically modeled as

$$\begin{aligned} i &= W(v_0)v = -\frac{1}{R_3}(1 - gv_0^2)v \\ C_0\frac{\mathrm{d}v_0}{\mathrm{d}t} &= -\frac{1}{R_1}v - \frac{1}{R_2}v_0 \end{aligned} \tag{1}$$

where $v$ and $i$ are the voltage and current at the input terminal of the memristor with memductance $W(v_0)$, respectively. $v_0$ is the voltage across the integral capacitor $C_0$, and $g$ is the total gain of the two multipliers $M_1$ and $M_2$.

The proposed circuit in Fig. 1(a) only has two dynamic elements, which are the capacitor $C_1$ and the active voltage-controlled memristor with memductance $W(v_0)$, corresponding to two state variables of $v_1$ and $v_0$, respectively. Thus, the proposed circuit in Fig. 1(a) can be modeled as

$$\begin{aligned} \frac{\mathrm{d}v_1}{\mathrm{d}t} &= \frac{v_s - v_1}{RC_1} + \frac{(1 - gv_0^2)v_1}{R_3C_1} \\ \frac{\mathrm{d}v_0}{\mathrm{d}t} &= -\frac{v_1}{R_1C_0} - \frac{v_0}{R_2C_0} \end{aligned} \tag{2}$$

where $v_s = A\sin(2\pi ft)$, and $A$ is the amplitude and $f$ indicates the frequency.

Taking advantage of the state equations modeled by (2), theoretical analyses and numerical simulations can be performed for the proposed non-autonomous memristive circuit. The typical circuit parameters in Fig. 1 are given as $R_1 = 8\ \mathrm{k\Omega}$, $R_2 = 4\ \mathrm{k\Omega}$, $R_3 = 1.4\ \mathrm{k\Omega}$, $R_4 = R_5 = 2\ \mathrm{k\Omega}$, $C_0 = 4.7\ \mathrm{nF}$, and $g = 0.1\ \mathrm{V}^{-2}$, $R = 2.6\ \mathrm{k\Omega}$, $C_1 = 6.8\ \mathrm{nF}$, $A = 2\ \mathrm{V}$, and $f = 7\ \mathrm{kHz}$.

## III. EQUILIBRIUM POINTS AND THEIR STABILITIES

By setting the left-hand side of model (2) to zero, an AC equilibrium point is easily obtained as $\tilde{S} = [-R_1\tilde{v}_0/R_2,\ \tilde{v}_0]$, in which $\tilde{v}_0$ can be numerically solved by

$$\tilde{v}_0^3 + p\tilde{v}_0 + q = 0 \tag{3}$$

where $p = (R_3 - R)/(gR)$ and $q = R_2R_3v_s/(gRR_1)$. The roots of (3) can be derived as

$$\begin{aligned} \tilde{v}_{01} = &\frac{-1 + \mathrm{j}\sqrt{3}}{2} \times \sqrt[3]{-\frac{q}{2} + \sqrt{\Delta}} \\ &+ \frac{-1 - \mathrm{j}\sqrt{3}}{2} \times \sqrt[3]{-\frac{q}{2} - \sqrt{\Delta}} \end{aligned} \tag{4}$$

$$\tilde{v}_{02} = \sqrt[3]{-\frac{q}{2} + \sqrt{\Delta}} + \sqrt[3]{-\frac{q}{2} - \sqrt{\Delta}} \tag{5}$$

$$\begin{aligned} \tilde{v}_{03} = &\frac{-1 - \mathrm{j}\sqrt{3}}{2} \times \sqrt[3]{-\frac{q}{2} + \sqrt{\Delta}} \\ &+ \frac{-1 + \mathrm{j}\sqrt{3}}{2} \times \sqrt[3]{-\frac{q}{2} - \sqrt{\Delta}} \end{aligned} \tag{6}$$

where $\Delta = (q/2)^2 + (p/3)^3$.

According to Cardan discriminant [30], when $\Delta > 0$, there exists a real root and two complex roots. Since the equilibrium point cannot be complex number, one equilibrium point is obtained from (5). However, when $\Delta = 0$, the two complex roots in (4) and (6) evolve to one real root, leading to the fact that two real roots appear in (3). Therefore, the proposed circuit has two equilibrium points. Similarly, when $\Delta < 0$,

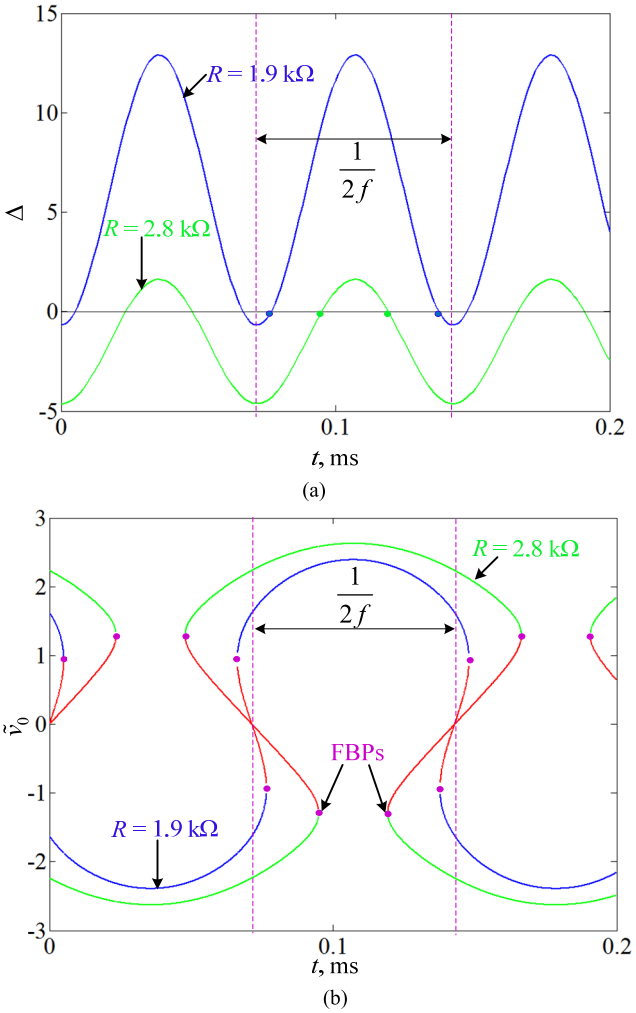


**FIGURE 2.** Cradan discriminant and equilibrium points vary with the evolution of the time under different resisters of $R$. (a) Cradan discriminant. (b) Number and values of equilibrium points.

there are three real roots in (3), which manifests that the proposed circuit has three equilibrium points and can be obtained from (4) – (6). For the specified circuit parameters, when $R$ varies from 1.9 kΩ to 2.8 kΩ, Cardan discriminant $\Delta$ and the number of equilibrium points with the evolution of the time are presented in Fig. 2. It can be seen from Fig. 2(a) that $\Delta$ is a periodic function of the time, and the sign of Cardan discriminant varies with the evolution of the time for each $R$, leading to the situation that the number of the equilibrium points changes from three to two, to one, to two and then to three in a half period of $v_s$ between the two dotted lines, as shown in Fig. 2(b).

By linearizing (2) around AC equilibrium points, the Jacobian matrix is given by

$$\mathbf{J} = \begin{bmatrix} -\dfrac{1}{RC_1} + \dfrac{1-g\tilde{v}_0^2}{R_3C_1} & \dfrac{-2gR_1\tilde{v}_0^2}{R_2R_3C_1} \\ -\dfrac{1}{R_1C_0} & -\dfrac{1}{R_2C_0} \end{bmatrix} \tag{7}$$

The characteristic equation associated with (7) is

$$\lambda^2 + \left(\frac{1}{RC_1} + \frac{1}{R_2C_0} - \frac{1-g\tilde{v}_0^2}{R_3C_1}\right)\lambda - \frac{1+g\tilde{v}_0^2}{R_2R_3C_1C_0} = 0 \tag{8}$$

Depending on the eigenvalues at the AC equilibrium points, the stabilities are determined by the sign of $\Delta$.

(i) When $\Delta < 0$, there are two pairs of complex conjugate roots with negative real parts and two real roots with opposite signs for the three equilibrium points.

(ii) When $\Delta = 0$, there are a pair of complex conjugate roots with negative real parts for one equilibrium point, and one zero root and one negative real root for the other.

(iii) When $\Delta > 0$, there is a pair of complex conjugate roots with negative real parts for the unique equilibrium point.

It can be summarized that two stable foci and one unstable saddle point exist for $\Delta < 0$, one stable focus and a fold bifurcation point (FBP) appear for $\Delta = 0$, and one stable focus remains for $\Delta > 0$. The red line denotes the unstable saddle point and the dots colored in cyan are FBPs in Fig. 2(b) specially. Note that the characteristic equation for FBP has one zero root and one negative real root.

In particular, when $v_s = 0$, the circuit in Fig. 1(a) is degraded into a second-order autonomous circuit. Thus, three DC equilibrium points for $R > R_3$ are yielded as

$$\begin{aligned} \bar{S}_0 &= (\bar{v}_1, \bar{v}_0) = (0, 0) \\ \bar{S}_\pm &= (\bar{v}_1, \bar{v}_0) = (\pm\frac{R_1}{R_2}\sqrt{\frac{R-R_3}{gR}}, \mp\sqrt{\frac{R-R_3}{gR}}) \end{aligned} \tag{9}$$

The stability of each DC equilibrium point is derived by solving the characteristic equation of (7) with $\bar{v}_0$. For the above given circuit parameters, the eigenvalues that characterize the stability of the DC equilibrium points are calculated as

$$\begin{aligned} \bar{S}_0 &: 48481, -53191 \\ \bar{S}_\pm &: -26596 \pm \mathrm{j}66710 \end{aligned} \tag{10}$$

which indicate that $\bar{S}_0$ is an unstable saddle point and $\bar{S}_\pm$ are two stable foci.

## IV. NUMERICALLY SIMULATED DYNAMICS

In our next work, typical circuit parameters given in Sec. II are employed and the initial states are taken as $v_1(0) = 0$ V and $v_0(0) = 0$ V. Furthermore, MATLAB ODE45 algorithm with time step $10^{-6}$ is utilized to draw bifurcation diagrams and phase portraits, and Wolf's method proposed in [31] is used to calculate Lyapunov exponents.

### A. DYNAMICS DEPENDING ON PARAMETER R

With $R$ increasing from 1.9 kΩ to 2.8 kΩ, single-parameter bifurcation diagram of the state variable $v_1$ and Lyapunov exponent spectra are presented, as shown in Fig. 3, from which the striking dynamical features including period, chaos, forward period doubling bifurcation (FPDB), reverse period doubling bifurcation (RPDB), tangent bifurcation (TB), and crisis scenarios (CSs) are observed. In the

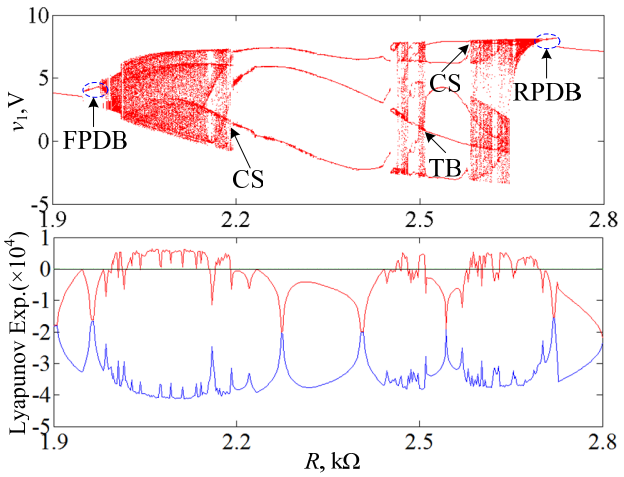


**FIGURE 3.** Single-parameter bifurcation diagram of $v_1$ and Lyapunov exponent spectrum with $R$ increasing.

considered parameter range of $R$, the dynamics starts from period-1, to period-2, to period-4, and then enters into chaos via the forward period doubling bifurcation route. Finally, the dynamics settles into period-1 via the reverse period doubling bifurcation. In the chaotic region, some periodic windows with different periodicities occur. When $1.9\ \text{k}\Omega \le R \le 1.98\ \text{k}\Omega$, $2.19\ \text{k}\Omega \le R \le 2.46\ \text{k}\Omega$, $2.51\ \text{k}\Omega \le R \le 2.58\ \text{k}\Omega$ or $2.69\ \text{k}\Omega \le R \le 2.8\ \text{k}\Omega$, the circuit shows various periodic behaviors with the first Lyapunov exponent less than zero. However, when $1.98\ \text{k}\Omega < R < 2.19\ \text{k}\Omega$, $2.46\ \text{k}\Omega < R < 2.51\ \text{k}\Omega$ or $2.58\ \text{k}\Omega < R < 2.69\ \text{k}\Omega$, the first Lyapunov exponent is mainly positive, but it is less than zero in some narrow parameter ranges, which indicates the occurrence of chaotic behaviors with periodic windows. Note that the crisis scenarios happen at $R = 2.19\ \text{k}\Omega$ and $R = 2.58\ \text{k}\Omega$ with sudden appearance or disappearance of the chaotic behaviors, and the tangent bifurcation occurs in a periodic window with the chaotic state suddenly turning into period-5 at $R = 2.51\ \text{k}\Omega$.

For the arbitrary values of $R$ and same initial states used in bifurcation diagrams, the trajectories of (2) on the $v_1 - v_0$ plane are numerically simulated, as shown in Fig. 4, respectively. The line colored in red denotes the trajectory of the unstable AC equilibrium point, and the lines colored in cyan denote the trajectories of stable AC equilibrium points. These numerical results just emulate the striking dynamical features of period and chaos emerging from the proposed circuit. From Fig. 4, it is found that the proposed circuit in Fig. 1 can generate chaotic attractors with three different topological structures, which implies that the proposed circuit is chaotic genuinely.

### B. BIFURCATION BEHAVIORS DEPENDING ON SINUSOIDAL SOURCE

With $f$ increasing from 4 kHz to 9 kHz and $A$ increasing from 1.5 V to 3.5 V, single-parameter bifurcation diagrams and Lyapunov exponent spectra are depicted in Figs. 5 and 6, respectively, which clearly indicate that the dynamical

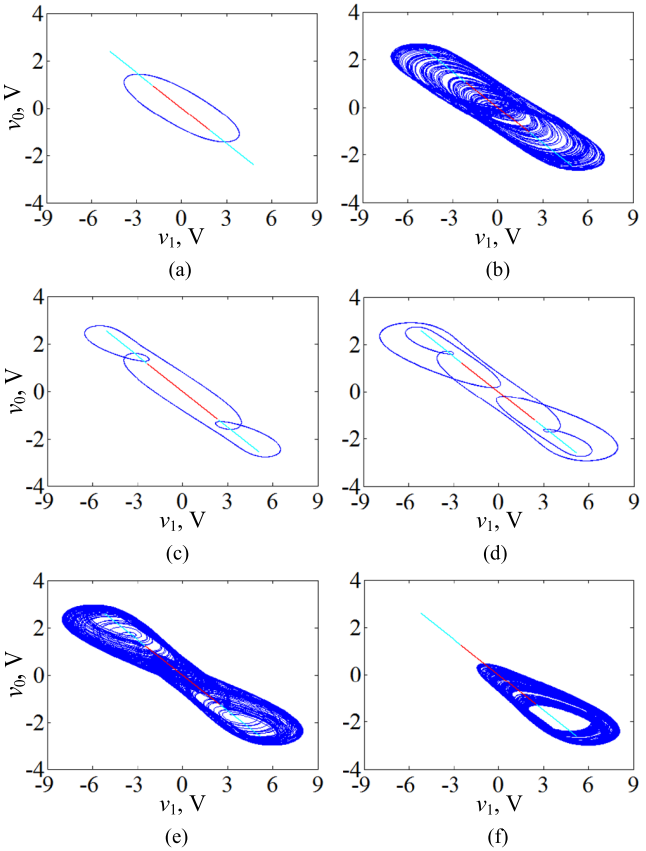


**FIGURE 4.** Numerical trajectories under different values of $R$ on the $v_1$–$v_0$ plane. (a) Period-1 limit cycle at $R = 1.9\ \text{k}\Omega$. (b) Chaotic attractor at $R = 2.1\ \text{k}\Omega$. (c) Period-3 limit cycle at $R = 2.4\ \text{k}\Omega$. (d) Period-5 limit cycle at $R = 2.55\ \text{k}\Omega$. (e) Double-scroll chaotic attractor ($R = 2.6\ \text{k}\Omega$). (f) Chaotic spiral attractor ($R = 2.66\ \text{k}\Omega$).

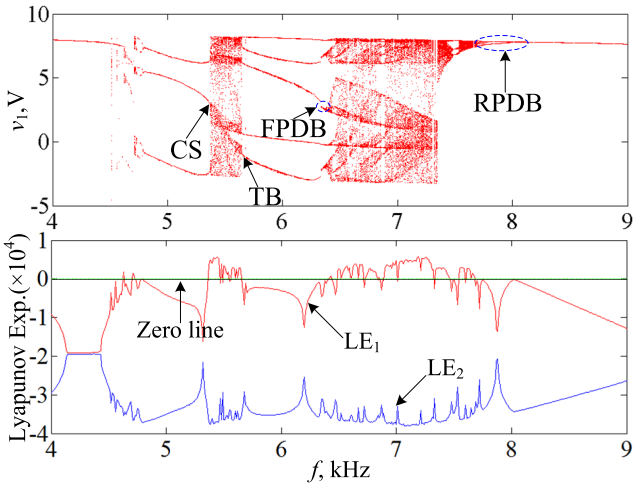


**FIGURE 5.** Single-parameter bifurcation diagram of $v_1$ and Lyapunov exponent spectrum with $f$ increasing.

behaviors exist in the proposed circuit, including period, chaos, periodic window, forward period doubling bifurcation (FPDB), reverse period doubling bifurcation (RPDB), tangent bifurcation (TB), crisis scenario (CS), and so on.

In Fig. 5, there are periodic behaviors with the first exponent less than zero and chaotic behaviors with positive first

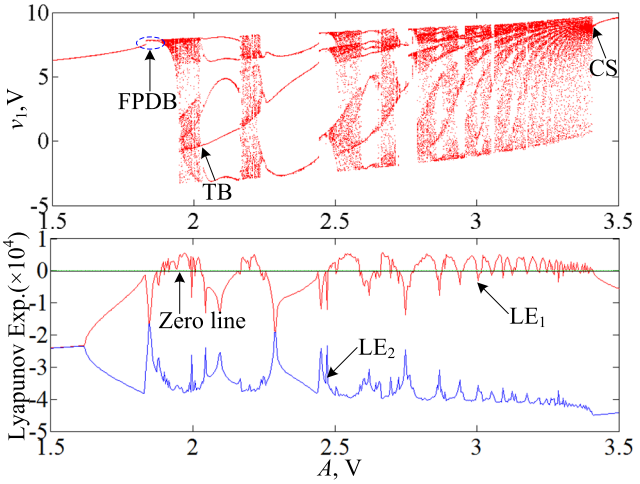


**FIGURE 6.** Single-parameter bifurcation diagram of $v_1$ and Lyapunov exponent spectrum with $A$ increasing.

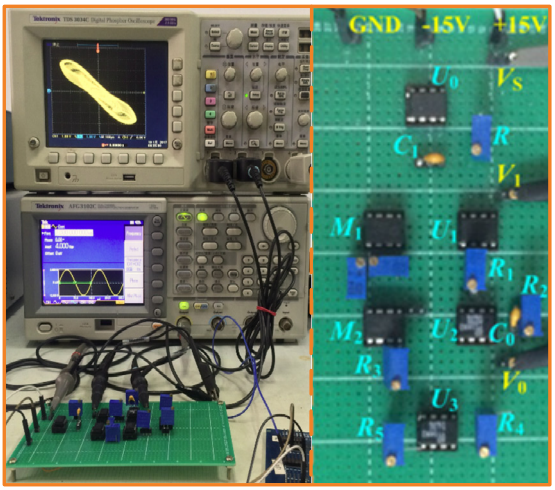


**FIGURE 7.** The experimental circuit of the proposed circuit, the left is a overviewed graph and the right is an enlargement of circuit breadboard.

Lyapunov exponent in the considered parameter range of the frequency $f$. The crisis scenario happens when $f = 5.37$ kHz and the tangent bifurcation occurs when $f = 5.65$ kHz. Nevertheless, when the amplitude is selected as a variable, the tangent bifurcation happens when $A = 2.02$ V and the crisis scenario occurs when $A = 3.41$ V, as shown in Fig. (6). It is interested that when $2.79\ \text{V} \leq A \leq 3.41$ V, the first Lyapunov exponent crosses the zero line alternately, which indicates that dynamical behaviors vary between periodic cycles and chaos as $A$ increases.

## V. HARDWARE EXPERIMENTS AND CAPTURED ATTRACTORS

With the circuit schematic in Fig. 1, an analogue electronic circuit is practically set up by some commercially available components, as shown in Fig. 7, where potentiometers and monolithic capacitors as well as operational amplifiers AD711KN and multipliers AD633JN with bipolar $\pm 15$ V supply are adopted. The circuit parameters used during

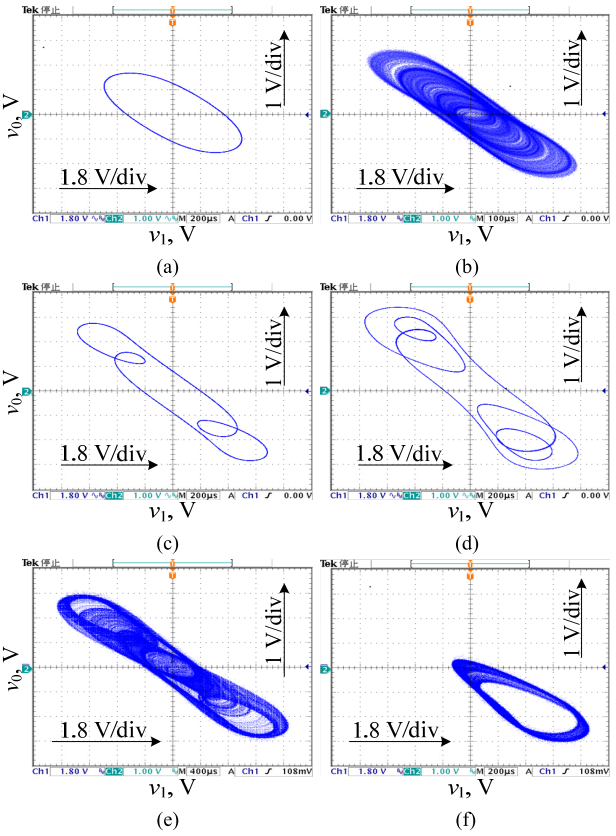


**FIGURE 8.** Attractors observed by digital oscilloscope under different values of $R$ in the $v_1$–$v_0$ plane. (a) Period-1 limit cycle at $R = 1.9$ kΩ. (b) Chaotic attractor at $R = 2.1$ kΩ. (c) Period-3 limit cycle at $R = 2.4$ kΩ. (d) Period-5 limit cycle at $R = 2.55$ kΩ. (e) Double-scroll chaotic attractor ($R = 2.6$ kΩ). (f) Chaotic spiral attractor ($R = 2.66$ kΩ).

numerical simulations are employed in hardware experiments and Tektronix AFG 3102C is taken as the sinusoidal voltage source. All of the resistors in our hardware experiments are replaced by precision potentiometers and their values are measured by Tonghui TH2816A Precision LCR Meter. Additionally, the experimental results are captured by a Tektronix TDS 3034C digital oscilloscope in XY mode with 1.8 V/div in X direction and 1 V/div in Y direction. Note that one auxiliary voltage follower circuit realized by an operation amplifier AD711KN $U_0$ is hired in experimental measurements to isolate the applied sinusoidal voltage source.

A precision potentiometer is utilized for the adjustable $R$ and its resistance is gradually tuned. For different values of $R$ used in numerical simulations, the attractors observed by the digital oscilloscope in the $v_1$–$v_0$ plane are shown in Fig. 8. Remark that ignoring the minor deviations caused by parasitic circuit parameters and active device non-idealities, the experimental results shown in Fig. 8 are well consistent with the numerical results in Fig. 4, which illustrates the existence of striking dynamics in the second-order non-autonomous inductor-free memristive chaotic circuit.

## VI. CONCLUSION

By driving a parallel memristor and capacitor filter with a sinusoidal voltage source, a simple second-order

non- autonomous inductor-free memristive chaotic circuit is presented in this paper. Numerical simulations and the corresponding hardware experiments are performed, which indicate that the simple circuit has dynamical behaviors of limit cycles with different periodicities and chaotic attractors with three different topological structures. It is notable that the dynamical behaviors must be induced by the time-evolutional equilibrium points. Specially, compared with the pioneering works of non-autonomous chaotic circuits, the significant features of the proposed memristive circuit are that the circuit only contains two dynamic elements and is an inductor-free realization with hardware gadget, which is suitable for IC design.

## REFERENCES

[1] L. O. Chua, "The fourth element," *Proc. IEEE*, vol. 100, no. 6, pp. 1920–1927, Jun. 2012.
[2] J. Ma, Z. Q. Chen, Z. L. Wang, and Q. Zhang, "A four-wing hyper-chaotic attractor generated from a 4-D memristive system with a line equilibrium," *Nonlinear Dyn.*, vol. 81, no. 3, pp. 1275–1288, Aug. 2015.
[3] I. Petráš, "Fractional-order memristor-based Chua's circuit," *IEEE Trans. Circuits Syst. II, Exp. Briefs*, vol. 57, no. 12, pp. 975–979, Dec. 2010.
[4] A. L. Fitch, D. Yu, H. H. Iu, and V. Sreeram, "Hyperchaos in a memristor-based modified canonical Chua's circuit," *Int. J. Bifurc. Chaos*, vol. 22, no. 6, pp. 1250133-1-1250133-8, Dec. 2012.
[5] L. Zhou, C. H. Wang, and L. L. Zhou, "Generating hyperchaotic multi-wing attractor in a 4D memristive circuit," *Nonlinear Dyn.*, vol. 85, no. 4, pp. 2653–2663, Aug. 2016.
[6] J. Kengne, Z. N. Tabekoueng, V. K. Tamba, and A. N. Negou, "Periodicity, chaos, and multiple attractors in a memristor-based Shinriki's circuit," *Chaos*, vol. 25, no. 10, pp. 103126-1-103126-10, Oct. 2015.
[7] Q. Xu, Y. Lin, B. C. Bao, and M. Chen, "Multiple attractors in a non-ideal active voltage-controlled memristor based Chua's circuit," *Chaos Solit. Fractals*, vol. 83, pp. 186–200, Feb. 2016.
[8] P. Saha, D. C. Saha, A. Ray, and A. R. Chowdhury, "Memristive non-linear system and hidden attractor," *Eur. Phys. J. Special Top.*, vol. 224, no. 8, pp. 1563–1574, Jul. 2015.
[9] B. C. Bao, Z. H. Ma, J. P. Xu, Z. Liu, and Q. Xu, "A simple memristor chaotic circuit with complex dynamics," *Int. J. Bifurc. Chaos*, vol. 21, no. 9, pp. 2629–2645, Sep. 2011.
[10] A. I. Ahamed and M. Lakshmanan, "Nonsmooth bifurcations, transient hyperchaos and hyperchaotic beats in a memristive Murali-Lakshmanan- Chua circuit," *Int. J. Bifurc. Chaos*, vol. 23, no. 6, pp. 1350098-1–1350098-28, Jun. 2013.
[11] B. Bao, P. Jiang, H. Wu, and F. Hu, "Complex transient dynamics in periodically forced memristive Chua's circuit," *Nonlinear Dyn.*, vol. 79, no. 4, pp. 2333–2343, Mar. 2015.
[12] A. I. Ahamed, K. Srinivasan, K. Murali, and M. Lakshmanan, "Observation of chaotic beats in a driven memristive Chua's circuit," *Int. J. Bifurc. Chaos*, vol. 21, no. 3, pp. 737–757, Mar. 2011.
[13] D. S. Yu, C. Y. Zheng, H. H. C. Iu, T. Fernando, and L. O. Chua, "A new circuit for emulating memristors using inductive coupling," *IEEE Access*, vol. 5, pp. 1284–1295, Jan. 2017.
[14] H. H. C. Iu, D. S. Yu, A. L. Fitch, V. Sreeram, and H. Chen, "Controlling chaos in a memristor based circuit using a twin-T notch filter," *IEEE Trans. Circuits Syst. I, Reg. Papers*, vol. 58, no. 6, pp. 1337–1344, Jun. 2011.
[15] H. G. Wu, B. C. Bao, Z. Liu, Q. Xu, and P. Jiang, "Chaotic and periodic bursting phenomena in a memristive Wien-bridge oscillator," *Nonlinear Dyn.*, vol. 83, no. 1, pp. 893–903, Jan. 2016.
[16] F. Corinto and A. Ascoli, "Memristive diode bridge with LCR filter," *Electron. Lett.*, vol. 48, no. 14, pp. 824–825, Jul. 2012.
[17] B. C. Bao, T. Jiang, Q. Xu, M. Chen, H. G. Wu, and Y. H. Hu, "Coexisting infinitely many attractors in active band-pass filter-based memristive circuit," *Nonlinear Dyn.*, vol. 86, no. 3, pp. 1711–1723, Aug. 2016.
[18] A. P. Kuznetsov, S. P. Kuznetsov, E. Mosekilde, and N. V. Stankevich, "Co-existing hidden attractors in a radio- physical system," *J. Phys. A, Math. Theor.*, vol. 48, no. 12, pp. 125101-1–125101-18, Mar. 2015.
[19] J. S. Pei, P. W. Joseph, D. T. Michael, F. M. Sami, and G. B. Francois, "Understanding memristors and memcapacitors in engineering mechanics applications," *Nonlinear Dyn.*, vol. 80, no. 1, pp. 457–489, Apr. 2015.
[20] S. Duan, X. Hu, L. Wang, S. Gao, and C. Li, "Hybrid memristor/RTD structure-based cellular neural networks with applications in image processing," *Neural Comput. Appl.*, vol. 25, no. 2, pp. 291–296, Aug. 2014.
[21] J. X. Zha, H. Huang, and Y. J. Liu, "A novel window function for memristor model with application in programming analog circuits," *IEEE Trans. Circuits Syst. II, Exp. Briefs*, vol. 63, no. 5, pp. 423–427, Mar. 2016.
[22] B. Arindam, "Small-signal neural models and their applications," *IEEE Trans. Biomed. Circuits Syst.*, vol. 6, no. 1, pp. 64–75, Feb. 2012.
[23] R. P. Jessica and J. C. Sprott, "Simple autonomous chaotic circuit," *IEEE Trans. Circuits Syst. II, Exp. Briefs*, vol. 57, no. 9, pp. 730–734, Sep. 2010.
[24] M. Gotz, U. Feldmann, and W. Schwarz, "Synthesis of higher dimensional Chua circuit," *IEEE Trans. Circuits Syst. I, Fundam. Theory Appl.*, vol. 40, no. 11, pp. 854–860, Nov. 1993.
[25] D. Premraj, K. Suresh, T. Banerjee, and K. Thamilmaran, "An experimental study of slow passage through Hopf and pitchfork bifurcations in a parametrically driven nonlinear oscillator," *Commun. Nonlinear Sci. Numer. Similat.*, vol. 37, pp. 212–221, May 2016.
[26] A. Arulgnanam, K. Thamilmaran, and M. Daniel, "Chaotic dynamics with high complexity in a simplified new nonautonomous nonlinear electronic circuit," *Chaos Solitons Fractals*, vol. 42, no. 4, pp. 2246–2253, Nov. 2009.
[27] T. Banerjee, "Single amplifier biquad based inductor-free Chua's circuit," *Nonlinear Dyn.*, vol. 68, no. 4, pp. 565–573, Jun. 2012.
[28] B. C. Bao, N. Wang, M. Chen, Q. Xu, and J. Wang, "Inductor-free simplified Chua's circuit only using two-op-amps-based realization," *Nonlinear Dyn.*, vol. 84, no. 2, pp. 511–525, Apr. 2016.
[29] B. Bao, N. Wang, Q. Xu, H. Wu, and Y. Hu, "A simple third-order memristive band pass filter chaotic circuit," *IEEE Trans. Circuits Syst. II, Exp. Briefs*, to be published, doi: 10.1109/TCSII.2016.2641008.
[30] C. Han, S. Yu, and G. Wang, "A sinusoidally driven lorenz system and circuit implementation," *Math. Prob. Eng.*, vol. 2015, May 2015, Art. no. 706902.
[31] A. Wolf, J. B. Swift, H. L. Swinney, and J. A. Vastano, "Determining Lyapunov exponents from a time series," *Phys. D, Nonlinear Phenom.*, vol. 16, no. 3, pp. 285–317, Jul. 1985.

**QUAN XU** was born in Lianyungang, China, in 1983. He received the B.S. degree in physics from the School of Huaiyin Teachers College, in 2005, and the M.S. and Ph.D. degrees in optical engineering from the University of Electronics Science and Technology of China, in 2011.

Since 2011, he has been a Teacher with Changzhou University, China. He is the author of more than 20 articles, and more than ten inventions. His research interest focuses on memristor and its applications, and memristive chaotic circuit/system.

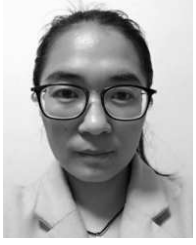

**QINLING ZHANG** was born in Taixing, China, in 1981. She received the B.S. degree in physics from the School of Huaiyin Teachers College, in 2005. She is currently pursuing the M.S. degree in computer application technology with Changzhou University.

Her research interest is mainly on the design of memristor equivalent circuit, and non-autonomous memristive chaotic circuit/system and their experimental measurement.

**BOCHENG BAO** received the B.S. and M.S. degrees in electronic engineering from the University of Electronics Science and Technology of China, Chengdu, China, in 1986 and 1989, respectively, and the Ph.D. degree from the Department of Electronic Engineering, Nanjing University of Science and Technology, Nanjing, China, in 2010. He has over 20 years experience in industry and has ever been in several enterprises serving as a Senior Engineer and a General Manager. From 2008 to 2011, he was a Professor with the School of Electrical and Information Engineering, Jiangsu Teachers University of Technology, Changzhou, China. He is currently a Professor with the School of Information Science and Engineering, Changzhou University, Changzhou. His research interests include bifurcation and chaos, analysis and simulation in power electronic circuits, and nonlinear circuits and systems.

**YIHUA HU** (M'13–SM'15) received the B.S. degree in electronical motor driver and the Ph.D. degree in power electronics and drives from the China University of Mining and Technology, Jiangsu, China, in 2003 and 2011, respectively. Between 2011 and 2013, he was with the College of Electrical Engineering, Zhejiang University, as a Post-Doctoral Fellow. Between 2012 and 2013, he was an Academic Visiting Scholar with the School of Electrical and Electronic Engineering, Newcastle University, Newcastle upon Tyne, U.K. Between 2013 and 2015, he was a Research Associate with the Power Electronics and Motor Drive Group, University of Strathclyde. Currently, he is a Lecturer with the Department of Electrical Engineering and Electronics, University of Liverpool. He has authored over 35 peer reviewed technical papers in leading journal. His research interests include PV generation system, power electronics converters and control, and electrical motor drives.